Journal of
Nanoscience and Nanotechnology
Vol. 12, 2496–2502, 2012

Direct Formation of Reusable $TiO_2/CoFe_2O_4$ Heterogeneous Photocatalytic Fibers via Two-Spinneret Electrospinning

Cong-Ju Li[1,*], Jiao-Na Wang[1], Bin Wang[1], Jian Ru Gong[2,*], and Zhang Lin[3]

[1] *Beijing Key Laboratory of Clothing Materials R&D and Assessment, Beijing Institute of Fashion Technology, Beijing 100029, P. R. China*
[2] *National Center for Nanoscience and Technology, China, 11 Zhongguancun Beiyitiao, Beijing 100190, P. R. China*
[3] *Fujian Institute of Research on the Structure of Matter, Chinese Academy of Sciences, Fujian 350002, P. R. China*

A reusable photocatalytic $TiO_2/CoFe_2O_4$ composite nanofiber was directly formed by using a vertical two-spinneret electrospinning process and sol–gel method, followed by heat treatment at 550 °C for 2 h. The high photocatalytic activity of the composite nanofibers depends on the good morphology of the fibers and the appropriate calcination temperature. The crystal structure and magnetic properties of the fibers were characterized by X-ray diffraction (XRD), scanning electron microscopy (SEM), energy dispersion spectroscopy (EDS), transmission electron microscope (TEM) and vibrating sample magnetometer (VSM). The photocatalytic activity of the $TiO_2/CoFe_2O_4$ fibers was investigated through ultraviolet-visible absorbance following the photo-oxidative decomposition of phenol. Meanwhile, the presence of $CoFe_2O_4$ not only broadens the response region of visible light, but also enhances the absorbance of UV light. Furthermore, these fibers displayed photocatalytic activity associated with magnetic activity of $CoFe_2O_4$ ferrites, allowing easy separated of the photocatalysts after the photo-oxidative process and effectively avoided the secondary pollution of the treated water.

Keywords: Nano Composites, Scanning/Transmission Electron Microscopy, Electrospinning, Photocatalytic Activity, Magnetic Properties.

RESEARCH ARTICLE

1. INTRODUCTION

Environmental pollution has increased more and more public concern nowadays. It is well-known that synthetic dyes cannot be removed from water via routine waste water treatment processes after being released from their manufacturing and application processes. In the past three decades, semiconductor heterogeneous photocatalysts, as one of the most advanced physicochemical catalysts, have been extensively investigated for solving existed environmental problems.[1–3] Among the semiconductor materials, titanium dioxide (TiO_2) is the most widely used catalyst for such applications because of its nontoxicity, strong oxidizing power, long-term stability against photo chemical corrosion, robustness under UV illumination and relative cheapness.[4–7]

In general, TiO_2 photocatalysts are in the form of either nanoparticles or thin films. Since the photocatalytic reactions take place on the catalysts' surface, the catalysts with a large specific surface area are expected to have high catalytic activities.[2] Nanoparticles have small and uniform particle size and large surface area.[8–9] But it is extremely difficult to remove the TiO_2 nanoparticles from water, leading to repollute the treated water again. Thin films are readily reused but have much less active surface area than nanoparticles.[10] Therefore, our work is concerned with direct formation of a new nano-structural TiO_2 fiber, which can be separated readily and exhibits superior catalytic performance. From the last 90 s, electrospun nanofibers have received a great deal of attentions. And their high surface-to-volume ratio and inherent porous structure make them very suitable to be used in efficient filtering systems, wound dressings, protective clothing, reinforcement, and so on.[11] In present work, an improved elelctrospinning

*Authors to whom correspondence should be addressed.

 1533-4880/2012/12/2496/007 doi:10.1166/jnn.2012.5812

process using vertical two-spinneret electrospinning was applied, and the two electrospun jets with positive and negative voltage attached with each other, so a cluster of fibers was generated because of the interaction of whipping and attractive electric forces.

In recent years, some researchers prepared nanoparticles with magnetic core and photoactive shell using magnetic granules and TiO_2, and proved that the composite nanoparticles could be easily separated by the magnetic field as a result of its magnetic property.[12–15] Among the magnetic nanomaterials, cobalt ferrite ($CoFe_2O_4$) has been widely studied due to its high electromagnetic performance, excellent chemical stability, mechanical hardness, and high cubic magnetocrystalline anisotropy.[16] Meanwhile, the preparation method is simple and economic. The composite nanoparticles had magnetic property and could be separated easily by the magnetic field.

In this work, the bicomponent $TiO_2/CoFe_2O_4$ photocatalytic and magnetic nanofibers can be prepared through an improved electrospinning process using vertical two-spinneret electrospinning, and the two electrospun fibers can mix with each other to directly form a heterogeneous fiber with at least two properties. In addition, the composite nanofibers have broadened the response region from UV light to visible light and can be recollected with a magnet for reuse in a photocatalytic process.

2. EXPERIMENTAL DETAILS

2.1. Materials

Cobalt (II) nitrate hexahydrate ($Co(NO_3)_2{\cdot}6H_2O$, 99.0%, A. R. Tientsin Fuchen Chemical Reagents Co.) and ferric (III) nitrate ninehydrate ($Fe(NO_3)_3{\cdot}9H_2O$, 98.5%, A. R. Tientsin Yingdaxigui Chemical Reagents Co.) were used as precursors. Citric acid monohydrate ($C_6H_8O_7{\cdot}H_2O$, 99.5%, Tientsin Yingdaxigui Chemical Reagents Co.) was chosen to be a chelating agent. Ammonia water ($NH_3{\cdot}H_2O$, 25%, A. R.) was from Tientsin Yingdaxigui Chemical Reagents Co. to adjust the pH value. Poly (vinyl pyrrolidone) (PVP, Mr = 10, 000, A. R. Tientsin Damao Chemical Reagents Co.) was dissolved in acetic acid (CH_3COOH, A. R. 99.5%, Beijing Chemical Works) as a spinning aid. Tetrabutyl titanate ($Ti[O(CH_2)_3CH_3]_4$, A. R. Beijing Xingjin Chemical Plant) was chosen as a Ti resource. PVP was dissolved in anhydrous alcohol (CH_3CH_2OH, A. R. Beijing Chemical Works) as another spinning aid. All these reagents were used as received without further purification.

2.2. Preparation of $TiO_2/CoFe_2O_4$ Fibers

The vertical two-spinneret electrospinning and sol–gel process conditions are based on our previous work.[17–18] The $CoFe_2O_4$ precursor solution was prepared by dissolving 1.000 g $Co(NO_3)_2{\cdot}6H_2O$, 2.776 g $Fe(NO_3)_3{\cdot}9H_2O$ and 1.980 g citric acid in 30 ml of deionized water. The molar ratio between cobalt and iron was 1:2. After dissolving the metal precursors, the value of pH was regulated to 5–6 with ammonia water ($NH_3{\cdot}H_2O$). The following evaporation of water at 60 °C resulted in the formation of the gel. PVP solution (22.2 wt%) was prepared using acetic acid (10.0 ml) as a solvent. The electrospinning positive solution was obtained by mixing PVP solution with cobalt ferrite gel (about 3.0 ml) under vigorous stirring for about 12 h.

PVP (4.000 g) solution was prepared using anhydrous alcohol (15.0 ml) as a solvent which was used as a negative precursor solution for electrospinning. Tetrabutyl titanate (1.0 ml) and acetic acid (1.0 ml) were gradually added into the above solution under vigorous stirring to form a Ti resource. The mixture was then kept stirring at room temperature for 12 h.

The prepared electrospinning solutions were loaded into two plastic tubes (8–9 mm in diameter). The electrospinning process was carried out using our home-made electrospinning system (Fig. 1). Two flat-vertical spinnerets were assembled with an interval labeled as d_1 of 6 cm. One was connected to a positive high-voltage (HV) supply (DW-D303-2AC, Tientsin Dongwen High Voltage Power Supply Plant) with +18 kV. Another one was connected to a negative high-voltage supply and the voltage was −4 kV. The distance between the needle tips and the collector was marked in Figure 1. The distance between the positive spinneret and the collector along the straight horizontal ($d_1 + d_2$) could be adjusted to about 15.0 cm and the vertical distance of two spinnerets is labeled as d_3 of 6 cm. All electrospinning processes were carried out at room temperature. The electrospun fibers were dried at 60 °C for 12 h in air. The dried fibers were calcined at 450–750 °C for 2 h in air to get $TiO_2/CoFe_2O_4$ fibers with a heating rate of 150 °C/h.

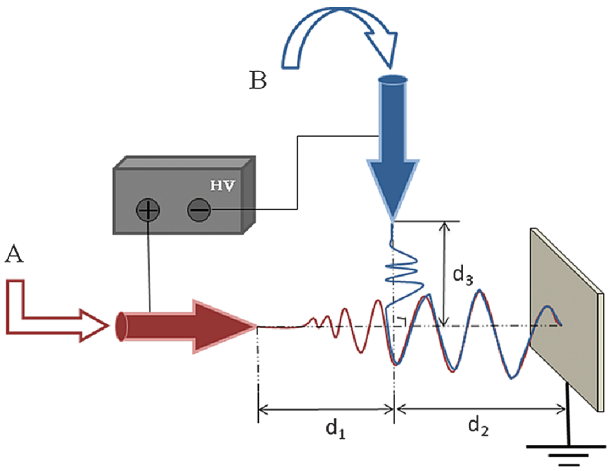

Fig. 1. The two-spinneret electrospinning process (d_1 = 6 cm, d_2 = 9 cm, and d_3 = 6 cm).

2.3. Characterization of $TiO_2/CoFe_2O_4$ Fibers

The morphology and structure of the products were characterized by X-ray diffraction (XRD, Rigaku D/MAX-IIIA, Japan) using Cu Kα radiation with $\lambda = 0.15406$ nm, and scanning electron microscopy (SEM, JSM-6360LV, Japan) equipped with energy dispersion spectroscopy (EDS) and transmission electron microscope (TEM, Tecnai G^2 20 S-TWIN). The magnetic properties (coercivity H_c, specific saturation magnetization M_s and specific remanent magnetization M_r) were performed at room temperature by a vibrating sample magnetometer (VSM, Lake Shore 7410) operating up to a maximum field of 20 kG.

2.4. Photocatalytic Activity Measurement

The bench-scale photoreactor system was composed of a cylindrical silica reactor and solar light with vertical irradiation. The light source was a 300 W Hg lamp (with UV light account for 40%, Shanghai Bilon Instruments Co., Ltd.) positioned inside a cylindrical Pyrex reactor and surrounded by a circulating water jacket for cooling. First 10.0 mg of phenol (C_6H_5OH, A. R. Tientsin Bodi Chemical Holding Co., Ltd.) were dispersed into 450.0 ml of deionized water. Then 25.0 mg of $TiO_2/CoFe_2O_4$ fibers were immersed into the phenol solution. Prior to irradiation, this reaction suspension was magnetically stirred in the dark for 12 h to ensure the establishment of an adsorption/desorption equilibrium of phenol on the catalyst surface before illumination. At a given irradiation time interval (30 min), 3.0 ml of aliquots were collected and centrifuged, in order to remove the solid catalyst particles. The absorbance of solution at 270 nm was measured to determine the concentration of phenol using a UV-vis spectrophotometer (TU-1901, Beijing Purkinje General Instrument Co., Ltd.) over the wavelength range of 190–800 nm.

3. RESULTS AND DISCUSSION

3.1. Crystal Structures of $TiO_2/CoFe_2O_4$ Composite Nanofibers

X-ray diffraction patterns for $TiO_2/CoFe_2O_4$ fibers prepared at various temperatures (450, 550, 650 and 750 °C) are shown in Figure 2. All of the main characteristic peaks are indexed as the anatase TiO_2 (PDF Card #84-1286), rutile TiO_2 (PDF Card #78-1508) and spinel $CoFe_2O_4$ (PDF Card #03-0864) in the standard data. The characteristic peaks are signed by α (25.3°, 37.9°, 48.1°, 54.0°, 55.1°, and 62.7°), β (27.4°, 36.1°, 41.3°, 54.4°, 56.7°, and 68.9°), and γ (30.2°, 35.5°, 57.2°, and 62.7°) as anatase TiO_2, rutile TiO_2 and spinel $CoFe_2O_4$, respectively.

As shown in Figure 2, with the gradual increase of calcination temperature (450–750 °C), the characteristic

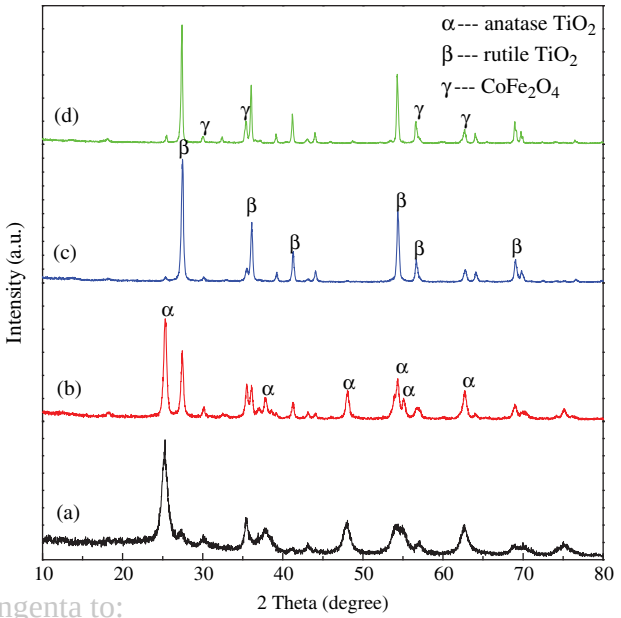

Fig. 2. XRD patterns for $TiO_2/CoFe_2O_4$ fibers at different calcination temperatures of (a) 450 °C, (b) 550 °C, (c) 650 °C, and (d) 750 °C.

peaks of anatase TiO_2 gradually disappear, and the characteristic peaks of rutile TiO_2 has gradually increased. This clearly indicates the polymorphic transformation from the anatase to the rutile phase occurred with the increase of the calcination temperature.[19–21] Compared with common monophase TiO_2 nanomaterials, composite nanocrystals there is a vectorial charge transfer at rutile/anatase heterostructured interfaces.[22] Therefore, the fibers calcined at 550 °C maybe possess better photocatalytic abilities.

As can be seen in Figure 2(b), when the calcination temperature reached 550 °C, there are a few slight peaks for spinel $CoFe_2O_4$ (PDF Card #03-0864), and the peaks become stronger with the gradual increasing of the calcination temperature. Compared with TiO_2, the characteristic peaks of $CoFe_2O_4$ are weaker. It is indicating that the content of $CoFe_2O_4$ phase in the calcined nanofibers is less than that of TiO_2 phase.

The average crystallite sizes of anatase TiO_2, rutile TiO_2 and spinel $CoFe_2O_4$ samples were calculated from X-ray line broadening using Scherrer's equation (i.e., $D = 0.89\lambda/(\beta\cos\theta)$, where λ is the wavelength of the X-ray radiation, θ is the diffraction angle and β is the full width at half maximum (FWHM)), and were found to be about 20.2, 22.4 and 20.2 nm, respectively.

3.2. Morphology and Surface Compositions of $TiO_2/CoFe_2O_4$ Composite Nanofibers

Figures 3(A and B) show the SEM images of the as-spun and calcined fibers respectively. The as-spun fibers ($TiO_2/CoFe_2O_4$/PVP) are continuous and smooth as shown in Figure 3(A). And PVP decompose during being calcined, so the calcined fibers ($TiO_2/CoFe_2O_4$) shrink and

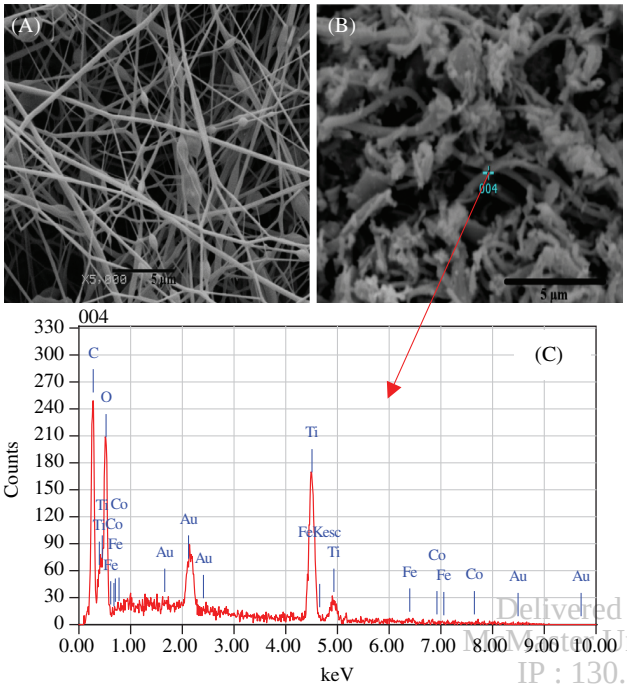

Fig. 3. Typical SEM images of the electrospun composite $TiO_2/CoFe_2O_4$ nanofibers: (A) as-spun and (B) calcined at 550 °C for 2 h; (C) Typical chemical analysis on selected spot of a single nanofiber.

seem to be shorter, which is shown in Figure 3(B). To some extent, the average diameters of the fibers also shrink after calcination due to the complete decomposition of PVP. Chemical analysis of the small nanofibers using EDS is shown in Figure 3(C). From the EDS results, it is shown that there are Ti, Co, Fe and O elements in a single fiber, and the contents of each element are displayed in Table I. From Table I, the determination of Ti/O and Fe/Co atomic ratio nearly confirms the presences of stoichiometric TiO_2 and $CoFe_2O_4$ (Ti/O atomic ratio of 0.55 and Fe/Co atomic ratio of 2.19). The EDS results associated with XRD patterns can illustrate that the resultant fibers are composited of TiO_2 and $CoFe_2O_4$.

Figures 4(A and B) show the TEM micrographs of the microstructure of the $TiO_2/CoFe_2O_4$ fiber and its lattice orientation. Figure 4(A) demonstrates that the surface of the fiber is slightly rough. Because $CoFe_2O_4$ is a magnetic material, and the absorption capacity of electron is much

Table I. EDS data of $TiO_2/CoFe_2O_4$ composite nanofibers calcined at 550 °C.

Element	Mass (%)	Atom (%)
C K	18.32	34.64
O K	28.61	40.61
Ti K	47.51	22.53
Fe K	3.76	1.53
Co L	1.81	0.70
Total	100.00	100.00

ZAF method standardless quantitative analysis. Fitting coefficient: 0.3435.

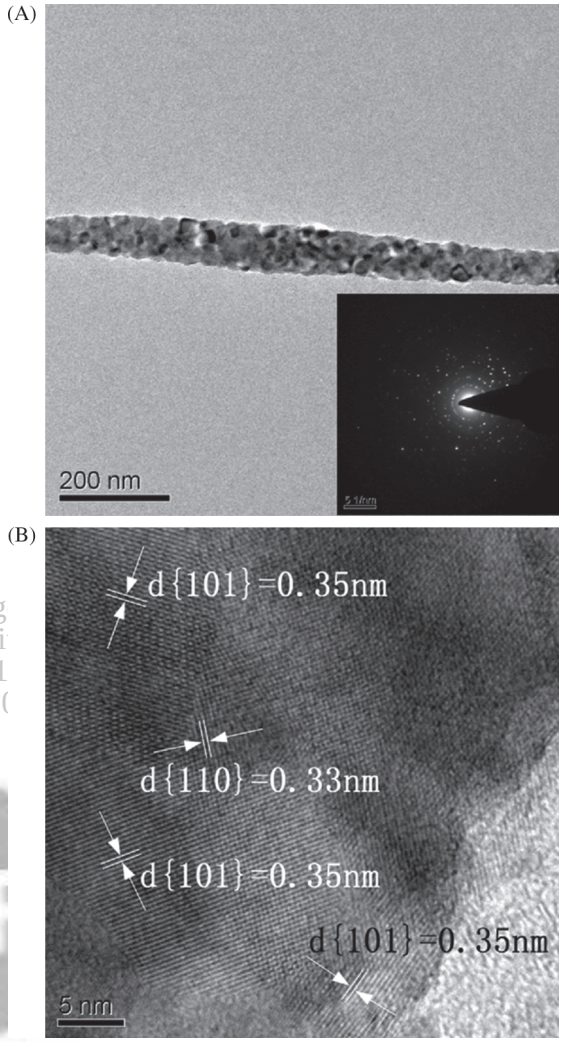

Fig. 4. TEM images of $TiO_2/CoFe_2O_4$ fibers calcined at 550 °C, (A) Low-resolution image (the inset figure is electron diffraction pattern) and (B) high-resolution image.

larger than that of TiO_2, the dark part represents $CoFe_2O_4$, while the light part is TiO_2 as shown in Figure 4(A).[23] $CoFe_2O_4$ and TiO_2 distribute along the axial direction of the fiber, which is benefit to the magnetically separable process and photocatalytic activity. The discontinuous diffraction rings in Electron diffraction pattern (ED) (Fig. 4(A) inset figure) display that this composite nanofiber is polycrystalline. Also anatase TiO_2 and rutile TiO_2 can be identified directly in the high-resolution TEM image of the nanofiber [Fig. 4(B)], which is evidenced by the interplanar distance of 0.35 nm related to (101) of anatase TiO_2 and 0.33 nm related to (110) of rutile TiO_2 respectively. Despite there is not any evidence to $CoFe_2O_4$ planes, the results of XRD and EDS can prove its existence obviously.

3.3. UV-Vis Diffuse Reflectance Spectra Analysis

Figure 5 gives the UV-vis diffuse reflectance spectra of Degussa P25 and $TiO_2/CoFe_2O_4$ composite nanofibers

RESEARCH ARTICLE

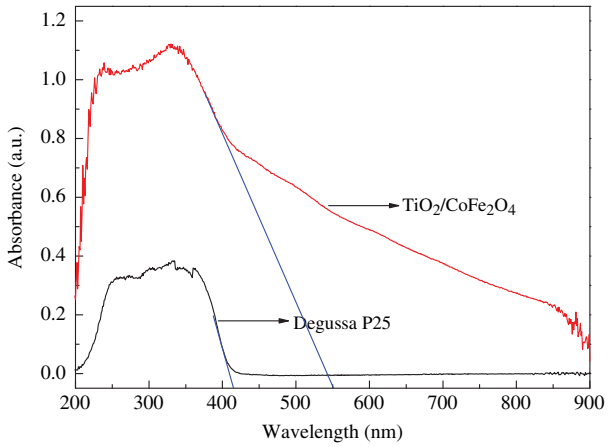

Fig. 5. The UV-vis diffuse reflectance spectra of Degussa P25 and $TiO_2/CoFe_2O_4$ fibers.

calcined at 550 °C for 2 h. It can be seen clearly that the catalyst has a significant red shift (indicated by the oblique lines) compared to P25, and the intensity of absorbance of the composite photocatalyst also significantly increases. The absorption edge of the composite photocatalyst has broadened to the visible light region, and this unusual optical red shift might be attributed to the following reasons:
(1) electrons are confined in a small volume due to the reduced particle size which would lead to a reduction in the gap;
(2) the increase of the internal pressure P ($P = 2\gamma/r$, where γ is the surface tension of the particle and r is the radius of the particle) arising from the reduction of particle size would induce the overlap to increase in the outer wave functions of the material, which makes the gap narrow.[24]

So this red shift might be attributed to the fact that the Fe^{3+} or/and Co^{2+} ions enter into the lattice structure of TiO_2 to replace Ti^{4+} ions, altering its crystal and electronic structures. The ionic radius of Ti^{4+} (0.68 Å), Fe^{3+} (0.64 Å) and Co^{2+} (0.65 Å) are almost the same, hence it is possible that Fe^{3+} or/and Co^{2+} ions occupy some of the lattice sites of TiO_2, forming an iron titanium solid solution.[25] The Fe/Co-modification could make the band gap become narrower and increase the response region of visible light because of the dopant serve as trapping sites for h^+ or e^- or both of them. In addition, the results could also be attributed to other structural differences, such as the particle geometry and fiber geometry.

3.4. Photocatalytic Degradation of Phenol

Figure 6(A) shows the photocatalytic activity of $TiO_2/CoFe_2O_4$ composite nanofibers which were calcined at different temperatures, and the degradation of reactive phenol under 300 W Hg lamp irradiation was investigated. It can be seen that the photocatalytic activity of $TiO_2/CoFe_2O_4$ composite nanofibers decreases with

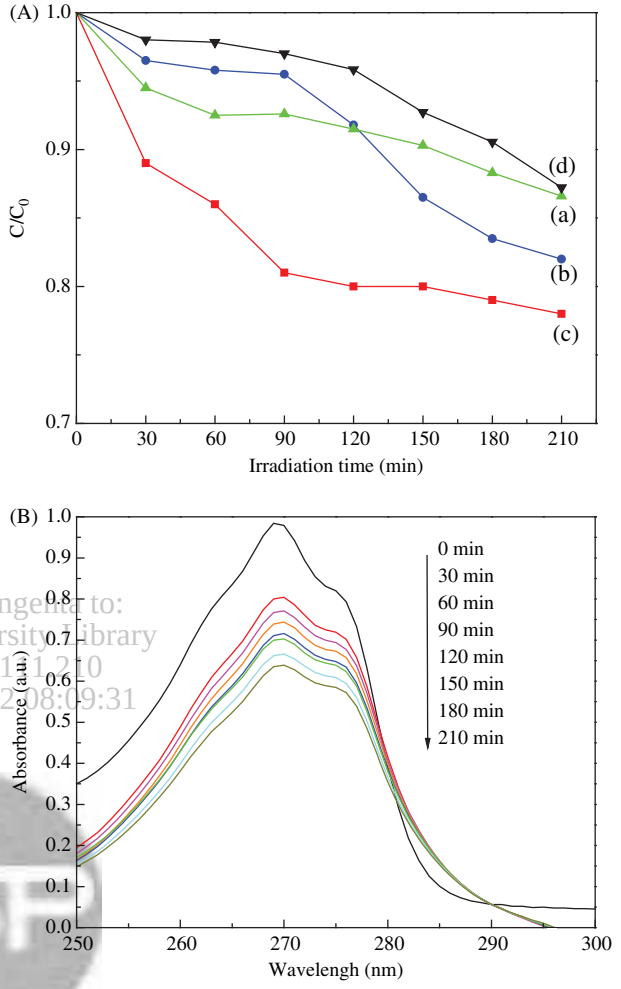

Fig. 6. (A) Photocatalytic activity of samples at various calcined temperatures: (a) 750 °C, (b) 650 °C, (c) 550 °C, and (d) 450 °C for phenol under UV light ($\lambda < 400$ nm) irradiation. (B) UV-vis spectra of phenol (10.0 mg, 450 ml) in aqueous dispersed $TiO_2/CoFe_2O_4$ (25.0 mg) calcined at 550 °C at different intervals of the irradiation time. Spectra from the top to the bottom refer to irradiation for 0, 30, 60, 90, 120, 150, 180, and 210 min, respectively.

increasing calcination temperature, from 550 °C to 750 °C, which leads to the polymorphic transition of titanium dioxide from anatase to rutile. Because of the effect of crystal form and crystallization degree of TiO_2, the photocatalytic activity is the poorest at 450 °C. The above result indicates that the optimal calcination temperature is 550 °C. Thermal treatment not only induced polymorphic transformation from anatase to rutile phase, but also led to changes in the crystallinity, surface area, and pore structure of TiO_2 particles.[19, 21]

On the one hand, generally speaking, TiO_2 in rutile form is less effective than the anatase form as a photocatalyst for the oxidation of most organic compounds. Anatase has a higher photocatalytic activity than rutile for several reasons.[26] One reason is that anatase has a larger band-gap (3.2 eV) than rutile (3.0 eV), so this provides anatase with a higher redox potential. Another reason is that anatase

has a higher area density of surface-bound hydroxyl groups (OH^-), slowing the recombination of photogenerated electron-hole pairs.[26] The hydroxyl groups are crucial for photocatalysis, since they react with photoexcited holes on the catalyst surface and produce hydroxyl radicals (OH·), which in turn are powerful oxidants in degrading organics in water.[27–28] On the other hand, with increasing calcination temperature, it has been established that the anatase phase structure, such as surface area, porosity and pore volume changed during the heat treatment process because of sintering. This result significantly impeded the photocatalytic degradation reaction, mainly because the reaction occurred on the surface of catalyst. All these factors may affect the photocatalytic activity, but it is difficult to estimate the separate contribution of each of them.

Compared with common monophase TiO_2 nanomaterials, composite nanocrystals possess better photocatalytic abilities because the vectorial charge transfer at rutile/anatase heterostructured interfaces is promoted.[22] In addition, Hurum et al. noted that rutile was photocatalytically active at longer wavelengths, and an enhancement may be observed depending on lighting conditions.[26] The above analysis explains the mechanism of the photocatalytic enhancement of the anatase-rutile mixture in our work.

3.5. Magnetic Properties and Separable Ability

The magnetic properties of pure $CoFe_2O_4$ and $TiO_2/CoFe_2O_4$ composite nanofibers were measured by VSM. Typical magnetization hysteresis loops are shown in Figure 7, and the values of H_c, M_s and M_r are summarised in Table II. Results reveal that TiO_2 greatly affects the magnetic properties of the $CoFe_2O_4$ fibers. Due to the presence of a non-magnetic TiO_2, the M_s and M_r values were less than that of pure $CoFe_2O_4$. This result is mainly attributed to the contribution of the concentration of the non-magnetic materials to the total sample volume.[29] However, the value of coercivity of $TiO_2/CoFe_2O_4$ fibers

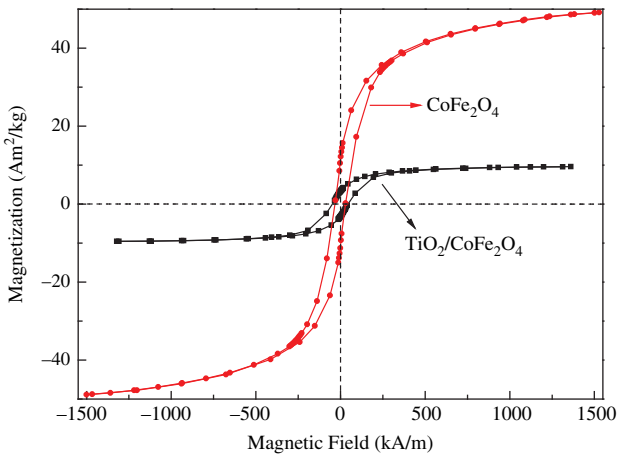

Fig. 7. The hystreesis loops for the $CoFe_2O_4$ and $TiO_2/CoFe_2O_4$ fibers calcined at 550 °C.

Table II. VSM data for different samples.

	H_c (kA/m)	M_r (Am^2/kg)	M_s (Am^2/kg)
Pure $CoFe_2O_4$	31.39	11.158	49.007
$TiO_2/CoFe_2O_4$	46.56	3.2408	9.5869

(46.56 kA/m) is higher than the pure $CoFe_2O_4$ fibers (31.39 kA/m), indicating the appearance of TiO_2 is benefit to the permanent magnetic properties.

Coercivity is an important parameter of magnetic materials to reflect the degree of permanent magnetism. It is related not only to the nature of the material itself, but also to the material microstructures such as grain size, grain shape and degree of irregularity, defects of grain surface, and coated condition. In this work, $CoFe_2O_4$ precursor was prepared by sol–gel method, which makes it fully dissolved and the size decreased. According to the adsorption characteristics of colloidal surface, $CoFe_2O_4$ particles preferentially adsorbed the same ion Co^{2+} and

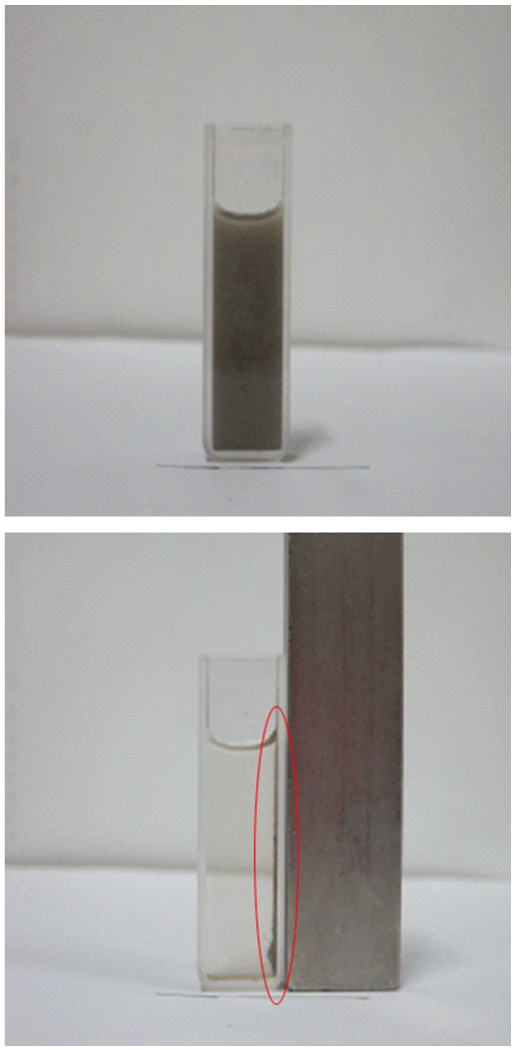

Fig. 8. Magnetic photocatalyst fibers were seperated from aqueous suspension by a storng permanent magnet (right): (A) before separation, (B) after separation.

Fe^{3+}, forming a cation shell. The repulsive interaction of shell can prevent agglomeration of $CoFe_2O_4$ particles and make it homodisperse.[30] Moreover, the presence of Ti^{4+} affects the grain shape and degree of irregularity, and defects of the grain surface. These reasons make the magnetic $CoFe_2O_4$ of $TiO_2/CoFe_2O_4$ composite nanofibers smaller than the pure $CoFe_2O_4$, and the magnetic composition distributes uniform in the electrospun nanofiber, so the coercivity of the $TiO_2/CoFe_2O_4$ composite nanofibers is higher than the pure $CoFe_2O_4$.

Finally, the predicted advantage of the heterogeneous photocatalysts is the association of photocatalytic and magnetic properties in a single fiber. A visual evaluation of the magnetic activity is seen in Figure 8, where the nanofibers are drawn towards the Nd-B magnet from an aqueous suspension in less than an hour, which also shows a homogeneous magnetic activity. In contrast, the aqueous suspension of P25 was precipitated after several hours. This is a profound advantage when the catalyst is used in practice, because separating ultra-fine catalyst nanoparticles is a serious problem, which impedes the application of TiO_2 nanoparticles at industrial scale.

4. CONCLUSION

In conclusion, reusable photocatalytic $TiO_2/CoFe_2O_4$ composite nanofibers with the average diameter of 100 nm were prepared successfully by two-vertical-spinneret electrospinning and sol–gel technology. The high photocatalytic activity of the composite nanofibers depends on the good morphology of the fibers and the appropriate calcination temperature. Meanwhile, the $TiO_2/CoFe_2O_4$ composite nanofibers not only enhance the absorbance of UV light, but also broaden the response region of visible light. Furthermore, these fibers can be separated with a magnet for reuse in a photocatalytic process, effectively avoiding the secondary pollution of the treated water. The two-vertical-spinneret electrospinning technology has increased the production efficiency and allows various kinds of composite nanofibers to be made. Therefore, it could be a versatile method for preparing reusable photocatalytic materials.

Acknowledgments: This study was partly supported by the Natural Science Foundation of China (Grant No. 51073005), the Beijing Natural Science Foundation (Grant Nos. 2112013, KZ201010012012), PHR (IHLB), the 973 Project (Grant No. 2010CB933501), Beijing Municipal Science and Technology Development Program (Grant No. Z111100066611004) and Textile Vision Science & Education Fund. And also supported by the financial support from National Basic Research Program of China (973 Program, No. 2011CB933401), National Natural Science Foundation of China (Nos. 21005023, 91123003), Special Presidential Foundation of Chinese Academy of Sciences and K. C. Wong Education Foundation, Hong Kong.

References and Notes

1. H. Xia, H. Zhuang, D. Xiao, and T. Zhang, *J. Alloys Compd.* 465, 328 **(2008)**.
2. J. Li, W. Ma, C. Chen, J. Zhao, H. Zhu, and X. Gao, *J. Mol. Catal. A: Chem.* 261, 131 **(2007)**.
3. M. A. Kanjwal, N. A. M. Barakat, F. A. Sheikh, M. S. Khil and H. Y. Kim, *Inter. J. Appl. Ceramic Technol.* 7, E54 **(2010)**.
4. W. Dong, C. W. Lee, X. Lu, Y. Sun, W. Hua, G. Zhuang, S. Zhang, J. Chen, H. Hou, and D. Zhao, *Appl. Catal. B: Environ.* 95, 197 **(2010)**.
5. C.-H. Huang, D. Gu, D. Zhao, and R.-A. Doong, *Chem. Mater.* 22, 1760 **(2010)**.
6. R. Liu, Y. Ren, Y. Shi, F. Zhang, L. Zhang, B. Tu, and D. Zhao, *Chem. Mater.* 20, 1140 **(2007)**.
7. Y.-H. Xu, H.-R. Chen, Z.-X. Zeng, and B. Lei, *Appl. Surf. Sci.* 252, 8565 **(2006)**.
8. F. Zhang, Y. Shi, X. Sun, D. Zhao, and G. D. Stucky, *Chem. Mater.* 21, 5237 **(2009)**.
9. X. Guo, Y. Deng, D. Gu, R. Che, and D. Zhao, *J. Mater. Chem.* 19, 6706 **(2009)**.
10. S. Eero, K. Marianna, L. Markku, and R. Mikko, *Nanotechnol.* 20, 035602 **(2009)**.
11. T. Lin, H. Wang, and X. Wang, *Adv. Mater.* 17, 2699 **(2005)**.
12. Y. S. Chung, S. B. Park, and D.-W. Kang, *Mater. Chem. Phy.* 86, 375 **(2004)**.
13. F. Chen, Y. Xie, J. Zhao, and G. Lu, *Chemosphere* 44, 1159 **(2001)**.
14. D. Beydoun, R. Amal, G. Low, and S. McEvoy, *J. Mol. Catal. A: Chem.* 180, 193 **(2002)**.
15. D. Beydoun and R. Amal, *Mater. Sci. Eng. B* 94, 71 **(2002)**.
16. Z. Zi, Y. Sun, X. Zhu, Z. Yang, J. Dai, and W. Song, *J. Magn. Magn. Mater.* 321, 1251 **(2009)**.
17. B. Zhang, C. Li, and M. Chang, *Polym. J* 41, 252 **(2009)**.
18. C.-J. Li and J.-N. Wang, *Mater. Lett.* 64, 586 **(2010)**.
19. Z. Wang, W. Cai, X. Hong, X. Zhao, F. Xu, and C. Cai, *Appl. Catal. B: Environ.* 57, 223 **(2005)**.
20. S. W. Lee, Y. U. Kim, S.-S. Choi, T. Y. Park, Y. L. Joo, and S. G. Lee, *Mater. Lett.* 61, 889 **(2007)**.
21. N. R. C. Fernandes Machado and V. S. Santana, *Catal. Today* 107, 595 **(2005)**.
22. C. Sun, N. Wang, S. Zhou, X. Hu, S. Zhou, and P. Chen, *Chem. Commun.* 3293 **(2008)**.
23. X. W. Zuo, P. Fei, C. L. Hu, B. T. Su, and Z. Q. Lei, *Chin. J. Inorg. Chem.* 25, 1233 **(2009)**.
24. Y. Liu, J. Ma, C. Dai, Z. Song, Y. Sun, J. Fang, C. Gao, and J. Zhao, *J. Am. Ceram. Soc.* 92, 2791 **(2009)**.
25. N. R. Mathews, M. A. C. Jacome, E. R. Morales, and J. A. T. Antonio, *physica status solidi c* 6, S219 **(2009)**.
26. K. Woan, G. Pyrgiotakis, and W. Sigmund, *Adv. Mater.* 21, 2233 **(2009)**.
27. E. Pelizzetti and C. Minero, *Electrochim. Acta* 38, 47 **(1993)**.
28. Z. Ding, G. Q. Lu, and P. F. Greenfield, *J. Phys. Chem. B* 104, 4815 **(2000)**.
29. M. Wan and W. Li, *J. Polym. Sci. Part A: Polym. Chem.* 35, 2129 **(1997)**.
30. A. Chen, H. Wang, and X. Li, *Synth. Met.* 145, 153 **(2004)**.

Received: 30 June 2011. Accepted: 21 September 2011.